Electronic Supplementary Material (ESI) for Chemical Communications.
This journal is © The Royal Society of Chemistry 2022

Electronic Supplementary Information

PNO: A Promising Deep-UV Nonlinear Optical Material with the Largest Second Harmonic Generation Effect

Congwei Xie[a†*], Abudukadi Tudi[b†], Artem R. Oganov[a*]

[a] Skolkovo Institute of Science and Technology, Skolkovo Innovation Center, 121205, Moscow, Russian Federation

[b] CAS Key Laboratory of Functional Materials and Devices for Special Environments, Xinjiang Technical Institute of Physics & Chemistry, CAS; Xinjiang Key Laboratory of Electronic Information Materials and Devices, 40-1 South Beijing Road, Urumqi 830011, China

[†]These authors contributed equally to this work.

Computational Details

Gaussian calculations: To obtain electronic and optical properties for a series of tetrahedral units, we performed DFT calculations using the Gaussian 09 software[1]. Based on the optimized geometry configurations, we used the B3LYP functional along with the 6-311G basis set to compute the highest occupied molecular orbital (HOMO)-lowest unoccupied molecular orbital (LUMO) gap Eg (HOMO-LUMO). In addition, at the same functional and basis set, we calculated UV-Vis spectrum for these units with time-dependent density functional theory (TD-DFT[2]) and derived their optical gaps Eg (TD-DFT). The polarizability α and the first hyperpolarizability β of these structure units were studied using CAM-B3LYP functional with 6-311G+(2d) basis set by adding polarization and diffuse functions[3]. We have also computed basis set dependence of β of these units for the CAM-B3LYP functional. As listed in Table S1, we can find that the present computational settings should be helpful to obtain reliable (hyper)polarizabilities. In the presence of an applied electric field, the energy of a system E is a function of the field strength $\boldsymbol{F}$ and (hyper)polarizabilities are defined as the coefficients in the Taylor series expansion of the energy in the external electric field, as expressed by the following equation[4,5]:

$$E(\boldsymbol{F}) = E(0) - \sum_i \mu_i F_i - \frac{1}{2!}\sum_i \sum_j \alpha_{ij} F_i F_j - \frac{1}{3!}\sum_i \sum_j \sum_k \beta_{ijk} F_i F_j F_k - \cdots$$

$$i, j, k = \{x, y, z\} \tag{1}$$

where $E(\boldsymbol{F})$ is the energy of a molecule under the electric field $\boldsymbol{F}$, $E(0)$ is the unperturbed energy of a free molecule, F_i is the vector component of the electric field in the i direction, and μ_i, α_{ij} and β_{ijk} are the dipole moment, linear polarizability and first hyperpolarizability, respectively. Here, each of the subscripts i, j and k denote the index of the Cartesian axes x, y, z, and a repeated subscript means a summation over the Cartesian indices x, y and z. In computational chemistry tools, α_{ij} and β_{ijk} are computed as the second and third-order derivatives of the energy (E) with respect to the applied field ($\boldsymbol{F}$) , respectively; these equations are as follows[4]:

$$\alpha_{ij} = -\left.\frac{\partial^2 E}{\partial F_i \partial F_j}\right|_{F=0} \tag{2}$$

$$\beta_{ijk} = -\left.\frac{\partial^3 E}{\partial F_i \partial F_j \partial F_k}\right|_{F=0} \tag{3}$$

This can be done numerically or analytically[1,6]. In this study, α_{ij} and β_{ijk} calculation at static frequency was computed numerically with the finite field approach (Freq = NRaman keyword). The stepsize of finite difference (F_i, $i = x, y, z$) was set to be 0.0033 au.

Based on the computed α and β tensor components at static frequency, we then derived polarizability anisotropy $\Delta\alpha$ and the mean first hyperpolarizability β_0 for each unit. The obtained results are presented in the Supporting Information (See Table S1). The polarizability anisotropy $\Delta\alpha$ and the mean first

hyperpolarizability β_0 was calculated using the following equations:

$$\Delta\alpha = \sqrt{\frac{1}{2}[(\alpha_{xx}-\alpha_{yy})^2+(\alpha_{xx}-\alpha_{zz})^2+(\alpha_{yy}-\alpha_{zz})^2+6(\alpha_{xy}{}^2+\alpha_{xz}{}^2+\alpha_{yz}{}^2)]} \quad (4)$$

$$\beta_0 = \left(\beta_x^2+\beta_y^2+\beta_z^2\right)^{\frac{1}{2}} \quad (5)$$

and

$$\beta_x = \beta_{xxx}+\beta_{xyy}+\beta_{xzz}$$
$$\beta_y = \beta_{yyy}+\beta_{xxy}+\beta_{yzz}$$
$$\beta_z = \beta_{zzz}+\beta_{xxz}+\beta_{yyz} \quad (6)$$

An external electric field can be either static or dynamic. The frequency dependence of (hyper)polarizabilities is known as dispersion. For [PN2O2] unit, we have also computed its frequency-dependent the first hyperpolarizability using the TD-DFT method with analytical derivatives (Polar = DCSHG keyword), as shown in Figure S1. It is found that the mean first hyperpolarizability β_0 can enhance drastically under the applied electric field.

Crystal structure predictions: The evolutionary algorithm as implemented in USPEX (Universal Structure Predictor: Evolutionary Xtallography) [7-9] code were used to explore deep-UV oxonitridophosphates. We performed variable-composition structure search for the P-N-O system with up to 36 atoms in the unit cell at zero temperature and ambient pressure. Those experimentally reported structures were used as seeds during the variable composition search. In each prediction, the first generation contains 120 structures produced randomly. Each subsequent generation contains 100 structures, of which 40% are produced by heredity, 20% softmutation, 20% transmutation operators and the rest of 20% random symmetric and random topological generators. For each structure produced by USPEX, with the help of VASP code[10], we performed first-principles total energy calculation and structural relaxation using the all-electron projector augmented wave (PAW)[11] method. The Perdew-Burke-Ernzerhof (PBE) functional[12] in the framework of generalized gradient approximation (GGA)[13] was adopted to describe the exchange-correlation potential - the valence electrons configurations of $3s^23p^3$, $2s^22p^3$ and $2s^22p^4$ were chosen for P, N and O, respectively. In these calculations, we used plane-wave kinetic energy cutoff of 600 eV and Γ-centred uniform k-point meshes with reciprocal-space resolution of $2\pi\times0.05$Å^{-1}.

First-principles properties calculations: For predicted PNO structures (PNO-I and PNO-II), the first-principles calculations are performed using CASTEP package[14] for obtaining their electronic band structure, optical properties and phonon dispersion spectrum. The ion-electron interactions are modeled by norm-conserving pseudopotentials for each atomic species with the following valence configurations: N $2s^22p^3$, O $2s^2$ $2p^4$, P $3s^23p^3$. The generalized gradient approximation (GGA) was adopted, and Perdew-Burke-Ernzerhof (PBE) functional was chosen to calculate the exchange-correlation potential. A series of computational parameters with high-precision are chosen for related calculations, including

a high plane-wave energy cutoff of 750eV and dense k-point meshes with reciprocal-space resolution of $2\pi\times0.03$Å^{-1}. The calculations of the linear optical performance were described in terms of the complex dielectric constant $\varepsilon(\omega) = \varepsilon_1(\omega) + i\varepsilon_2(\omega)$. The imaginary part $\varepsilon_2(\omega)$ of the dielectric function $\varepsilon(\omega)$ was calculated by using momentum matrix elements between the occupied and unoccupied electronic states:

$$\varepsilon_2(\hbar\omega) = \frac{2e^2\pi}{\Omega\varepsilon_0}\sum_{kcv}\left|\langle\psi_k^C|\hat{u}\cdot r|\psi_k^C\rangle\right|^2\delta\left[E_k^c - E_k^v\right] \tag{7}$$

Here Ω is the unit cell volume, v and c represent the valence band (VB) and conduction band (CB), ω and $\hat{u}$ are the frequency and the unit vector in the polarization direction of the incident light. Under the periodic boundary condition, $\left|\langle\psi_k^C|\hat{u}\cdot r|\psi_k^C\rangle\right|$ is the transition matrix element between the VB and the CB at a specific k point in the first Brillouin zone. The real part $\varepsilon_1(\omega)$ can be obtained from the imaginary part $\varepsilon_2(\omega)$ using the Kramers-Kronig transformation. The refractive indexes $n(\omega)$ and birefringence $\Delta n(\omega)$ can be obtained from the complex dielectric function. For achieving the phase-matching (PM) output in the ultraviolet region, a sufficiently large birefringence is needed. For the SHG process, it can realize the phase-matching SHG conditions only when the refractive indices of the fundamental wave and second-harmonic wave are equal: $n(2\lambda_{PM}) = n(\lambda_{PM})$, where λ_{PM} is the shortest SHG output wavelength.

The SHG coefficients were calculated using the so-called length-gauge formalism derived by Aversa and Sipe.[15] At zero frequency, the static second-order nonlinear susceptibilities can be ascribed to the virtual hole (VH) and virtual electron (VE) processes:[16,17]

$$\chi_{\alpha\beta\gamma}^{(2)} = \chi_{\alpha\beta\gamma}^{(2)}(\mathrm{VE}) + \chi_{\alpha\beta\gamma}^{(2)}(\mathrm{VH}) \tag{8}$$

Where $\chi_{\alpha\beta\gamma}^{(2)}(\mathrm{VE})$ and $\chi_{\alpha\beta\gamma}^{(2)}(\mathrm{VH})$ are computed using the following formulas:

$$\chi_{\alpha\beta\gamma}^{(2)}(\mathrm{VE}) = \frac{e^3}{2\hbar^2m^3}\sum_{vcc'}\int\frac{d^3k}{4\pi^3}P(\alpha\beta\gamma)\,\mathrm{Im}[p_{cv}^{\alpha}p_{cc'}^{\beta}p_{c'v}^{\gamma}]\times\left(\frac{1}{\omega_{cv}^3\omega_{vc'}^2}+\frac{2}{\omega_{vc}^4\omega_{c'v}^2}\right) \tag{9}$$

$$\chi_{\alpha\beta\gamma}^{(2)}(\mathrm{VH}) = \frac{e^3}{2\hbar^2m^3}\sum_{vv'c}\int\frac{d^3k}{4\pi^3}P(\alpha\beta\gamma)\,\mathrm{Im}[p_{vv'}^{\alpha}p_{v'c}^{\beta}p_{cv}^{\gamma}]\times\left(\frac{1}{\omega_{cv}^3\omega_{v'c}^2}+\frac{2}{\omega_{vc}^4\omega_{cv'}^2}\right) \tag{10}$$

Here, α, β, and γ are the Cartesian components; v / v' and c / c' denote the VBs and CBs; $P(\alpha\beta\gamma)$, $\hbar\omega_{ij}$, and p_{ij}^{α} refer to the full permutation, band energy difference, and momentum matrix elements, respectively. Accordingly, the SHG coefficient d_{ij} is determined by the transform from ($d_{i\beta\gamma}=1/2\chi_{i\beta\gamma}$) with the following subscript relationship between $\beta\gamma$ and j: 11 → 1; 22 → 2; 33 → 3; 23, 32 → 4; 13, 31 → 5; and 12, 21 → 6. The frequency-dependent SHG coefficients were calculated by ABINIT package.[18-20]

The hybrid functional (HSE06) as implemented in the PWmat code[21] was used to obtain more accurate band gaps (Eg-HSE), which has been shown to be consistent with experimental results. The number of empty bands needed to achieve converging results for the optical properties was set at three times the

number of VBs. The optical properties are calculated by the scissors-corrected GGA method, where the scissors operator is set as the energy difference between the Eg-HSE and Eg-GGA.

The elastic constants, directly related to the mechanical stability of a structure, were calculated by VASP code. For a mechanically stable structure with a given symmetry, its elastic constants should satisfy the corresponding stability criteria.[22] The mechanical properties (bulk modulus B and shear modulus G) of a material were evaluated using the Voigt-Reuss-Hill averaging scheme.[23,24] With B and G, the Vickers hardness H_V of a material can be obtained according to the Chen-Niu and Efim-Oganov empirical models.[25-27] Based on elastic constants, we can also evaluate lattice thermal conductivity and the minimum thermal conductivity at high temperature for a material by using the empirical Slack model and Clarke model, respectively.[28,29]

A comparison of SHG coefficients: PNO vs. KDP

In general, for most of experimentally synthesized NLO materials, their SHG coefficients will be preferentially measured with a laser of photon energy (1.17 eV). It has been reported that SHG coefficients of NLO materials generally slowly increase up to half the band gap.[30,31] And thus the computed static SHG coefficients are often used to compare with the experimental values.[31] For the well-known KDP, its SHG coefficient (d_{36}) calculated at zero frequency is 0.40 pm/V which is quite close to its experimental value (0.39 pm/V @ 1.17 eV). Using the same simulation method, we here computed the static SHG coefficients for PNO-I and PNO-II – it shows that the largest static SHG coefficients of these two structures (2.33~3.44 pm/V) are much larger than that of well-known KDP (0.40 pm/V). We have also computed frequency-dependent SHG responses for PNO-I, PNO-II and KDP. At photon energy equals to 1.17 eV, the maximum SHG coefficients for these three compounds are all comparable to their static ones (see Fig. S4 in the supporting information). It is also shown that PNO-I and PNO-II always have much stronger SHG response than KDP at all photon energy range (0 – 6 eV). We notice that there is a rough trend that the NLO materials with large bandgap will have small SHG response. Considering that PNO compounds have comparable bandgap (6.6 eV) with that of KDP (7.16 eV), it seems to be abnormal that PNO compounds have much higher SHG values than that of KDP. This can be explained by the big difference of the first hyperpolarizability between [PO4] and [PN2O2] units. As shown in Figure 1, [PN2O2] unit has a much higher hyperpolarizability than that of [PO4], suggesting that compounds containing [PN2O2] unit can have much higher SHG response that those containing [PO4] unit.

Table S1 The mean first hyperpolarizability (β_0, in a.u., 1 au = 3.20636 $\times 10^{-53}$ $C^3m^3J^{-2}$) computed for several different units using the CAM-B3LYP functional with different basis sets

Structure Units	β_0						
	6-311G	6-311G (d)	6-311G (2d)	6-311G (3d)	6-311G +(d)	6-311G +(2d)	6-311G +(3d)
[PO2F2]	8.9	0.1	3.7	3.8	34.9	42.5	41.9
[PO3F]	25.1	16.5	16.5	15.9	63.4	76.9	62.6
[SiO2F2]	22.6	26.1	20.1	24.2	22.3	28.8	37.4
[SiO3F]	9.2	6.4	6.0	1.2	166.7	130.8	490.1
[SiOF3]	45.3	51.0	42.7	44.5	12.6	15.9	33.6
[SiO3N]	430.9	397.4	340.8	452.4	1496.7	3564.7	-
[SiO2N2]	494.8	460.6	402.8	491.7	1152.0	1128.3	1182.8
[SiON3]	509.3	477.2	406.7	380.5	-	2950.4	2880.7
[PO3N]	101.1	103.4	78.5	69.9	932.4	925.5	815.8
[PO2N2]	124.6	130.0	100.4	91.6	1737.7	1698.4	1798.3
[PON3]	108.5	114.1	89.0	75.2	2660.6	1991.6	1655.9

Table S2 Computed HOMO–LUMO and TD-DFT gaps (Eg, in eV), polarizability anisotropy ($\Delta\alpha$, in a.u., 1 au = 1.6488 $\times 10^{-41}$ $C^2m^2J^{-1}$) and the mean first hyperpolarizability (β_0, in a.u., 1 au = 3.20636 $\times 10^{-53}$ $C^3m^3J^{-2}$) for several different units

Structure Units	Eg (HUMO-LUMO) (eV)	Eg (TD-DFT) (eV)	$\Delta\alpha$ (a.u.)	β_0 (a.u.)
[PN4]	4.69	4.37	0	0
[PNO3]	6.17	5.01	11.9	925.5
[PN2O2]	5.22	4.18	35.6	1698.4
[PN3O]	4.72	3.65	26.6	1991.6
[PO4]	8.28	7.43	0	0
[PO2F2]	9.17	8.25	6.7	42.5
[PO3F]	8.53	7.91	6.0	76.9
[SiN4]	3.94	3.47	0	0
[SiNO3]	4.08	3.11	77.3	3564.7
[SiN2O2]	3.60	2.59	30.1	1128.3
[SiN3O]	3.45	2.45	62.7	2950.4
[SiO4]	6.45	5.76	0	0
[SiOF3]	8.64	7.61	4.5	15.9
[SiO2F2]	7.91	6.74	7.0	8.7
[SiO3F]	6.65	5.88	8.8	130.8

Table S3 Structural and thermodynamical information of ten predicted PNO structures

Compound	Space groups	E above hull (eV/atom)	Density (g/cm^3)
PNO-I	$I2_12_12_1$	0	2.61
PNO-II	Cc	0.001	2.59
PNO-III	$P2$	0.003	2.58
PNO-IV	$R3$	0.012	2.46
PNO-V	$Pna2_1$	0.013	2.61
PNO-VI	$P2_12_12_1$	0.017	2.64
PNO-VII	P-1	0.024	2.77
PNO-VIII	$Ima2$	0.030	2.46
PNO-IX	$C2$	0.031	2.31
PNO-X	$P3_2$	0.040	2.91

Table S4 Mechanical and thermal properties of PNO-I and PNO-II

Compound	Is mechanically Stable?	Bulk modulus (GPa)	Shear modulus (GPa)	Vickers hardness (GPa) Chen-Niu	Vickers hardness (GPa) Efim-Oganov	Lattice thermal conductivity at 300 K ($W\ m^{-1}\ K^{-1}$)	The minimum thermal conductivity ($W\ m^{-1}\ K^{-1}$)
PNO-I	Yes	51.5	54.2	18.9	9.6	26.3	1.2
PNO-II	Yes	51.8	53.2	18.1	10.0	24.7	1.2

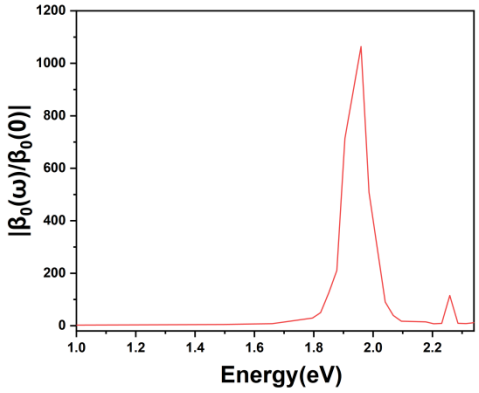

Fig. S1 The simulated frequency-dependent hyperpolarizability response for [PN2O2] unit. $\beta_0(-2w, w, w)$ is the mean first hyperpolarizability at applied field w (in eV) and $\beta_0(0, 0, 0)$ is the static mean first hyperpolarizability

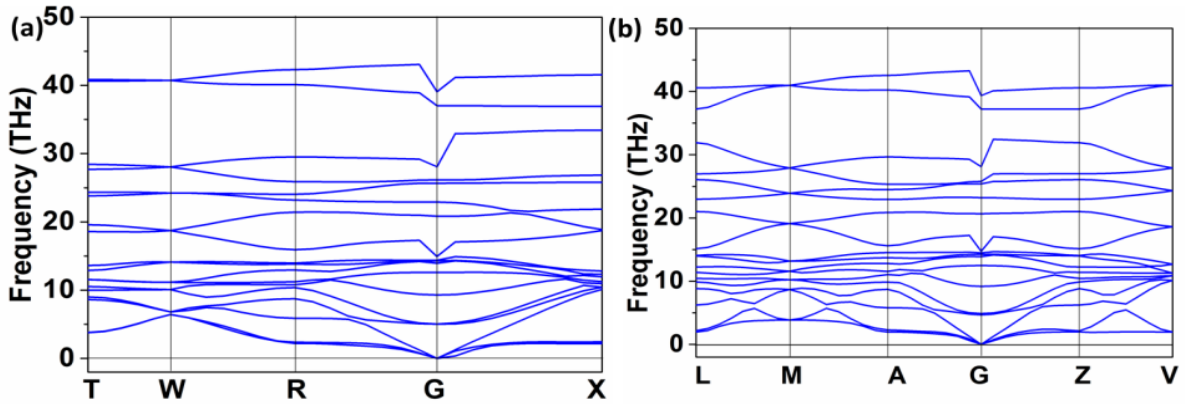

Fig. S2 Phonon dispersion spectra of (a) PNO-I, (b) PNO-II

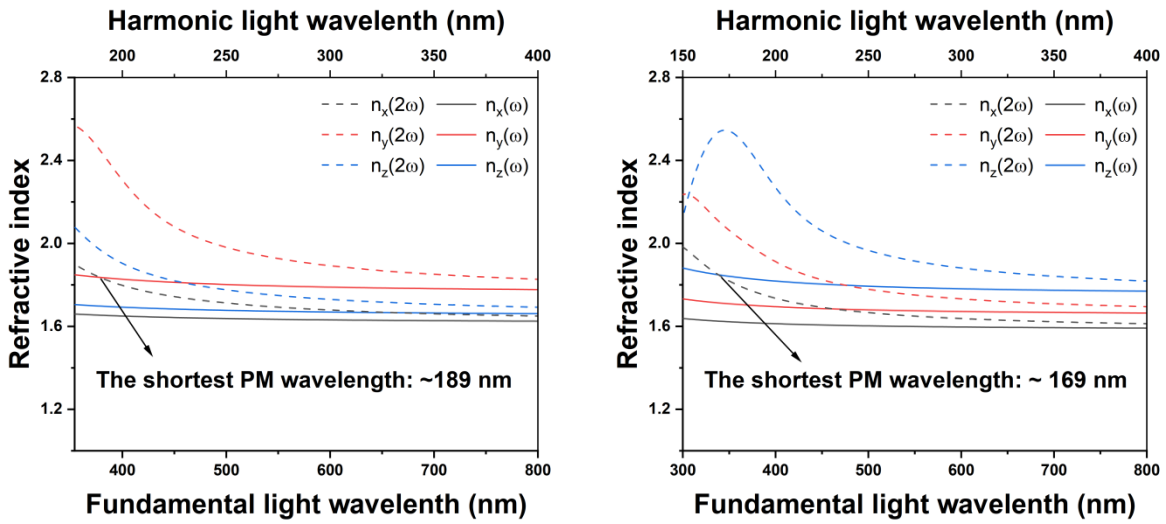

Fig. S3 Computed dispersion curves for both ordinary and extraordinary indices of refraction for PNO-I (left) and PNO-II (right)

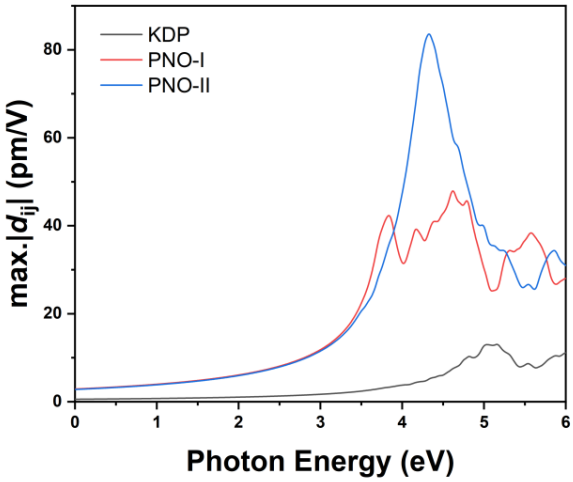

Fig. S4 The simulated frequency-dependent SHG response for bulk PNO-I,PNO-II and KDP compounds

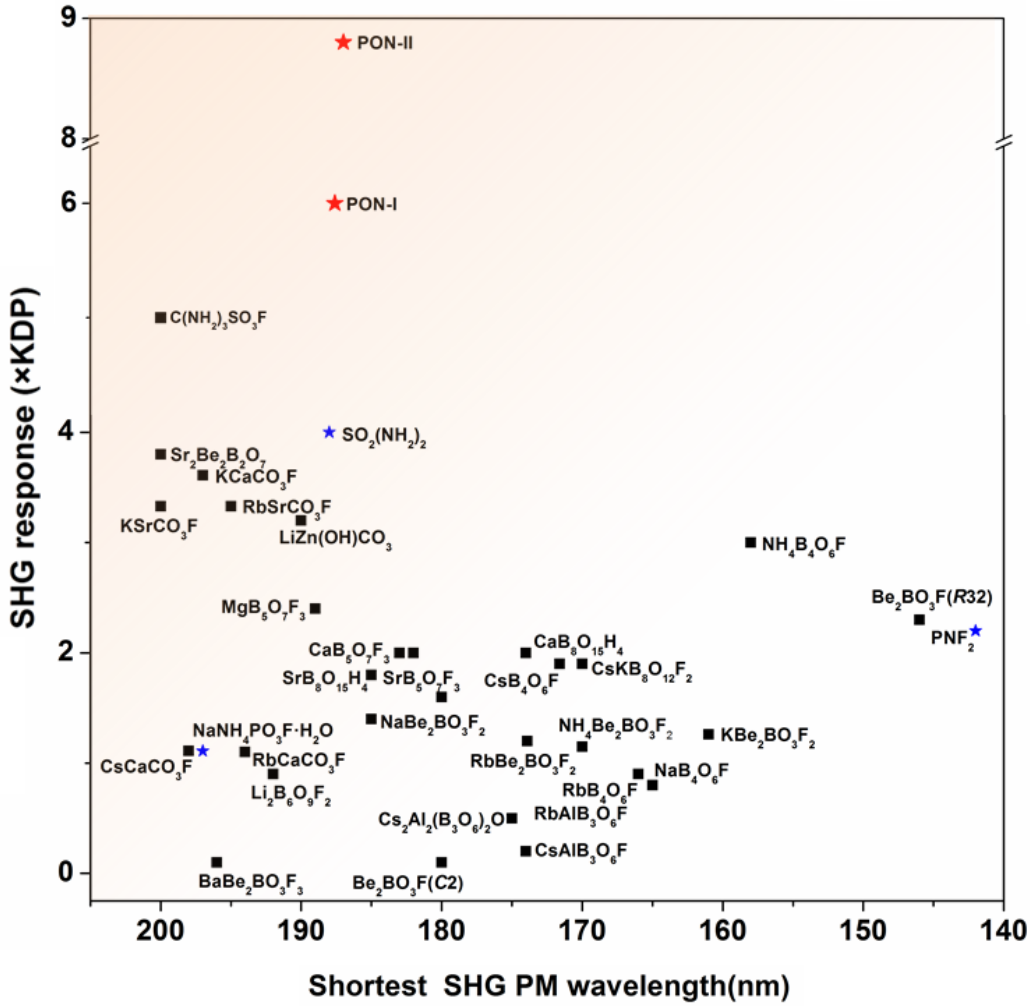

Fig. S5 The SHG response and shortest SHG phase-matching wavelengths of all the available experimentally obtained deep-UV NLO materials and PNO. π-conjugated systems are denoted by squares and non-π-conjugated stars

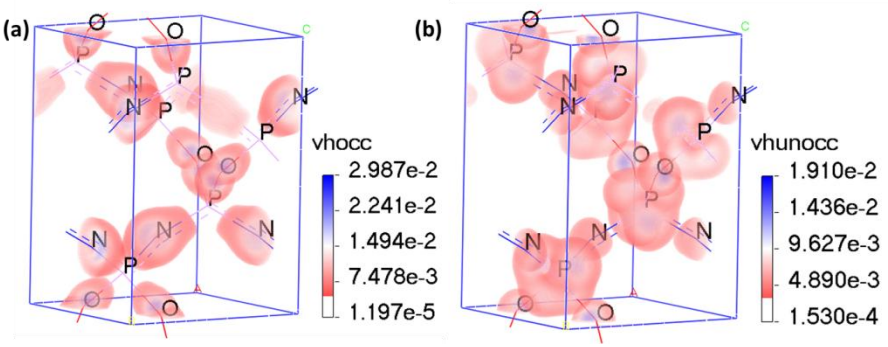

Fig. S6 SHG-density of PNO-I (a) VH occupied states, (b)VH unoccupied states

References

[1] M. J. Frisch, G. W. Trucks, H. B. Schlegel, G. E. Scuseria, M. A. Robb, J. R. Cheeseman, G. Scalmani, V. Barone, B. Mennucci, G. A. Petersson, H. Nakatsuji, M. Caricato, X. Li, H. P. Hratchian, A. F. Izmaylov, J. Bloino, G. Zheng, J. L. Sonnenberg, M. Hada, M. Ehara, K. Toyota, R. Fukuda, J. Hasegawa, M. Ishida, T. Nakajima, Y. Honda, O. Kitao, H. Nakai, T. Vreven, J. A. Montgomery, Jr. , J. E. Peralta, F. Ogliaro, M. Bearpark, J. J. Heyd, E. Brothers, K. N. Kudin, V. N. Staroverov, R. Kobayashi, J. Normand, K. Raghavachari, A. Rendell, J. C. Burant, S. S. Iyengar, J. Tomasi, M. Cossi, N. Rega, J. M. Millam, M. Klene, J. E. Knox, J. B. Cross, V. Bakken, C. Adamo, J. Jaramillo, R. Gomperts, R. E. Stratmann, O. Yazyev, A. J. Austin, R. Cammi, C. Pomelli, J. W. Ochterski, R. L. Martin, K. Morokuma, V. G. Zakrzewski, G. A. Voth, P. Salvador, J. J. Dannenberg, S. Dapprich, A. D. Daniels, O. Farkas, J. B. Foresman, J. V. Ortiz, J. Cioslowski, D. J. Fox, Gaussian 09, Revision A.02, Gaussian, Inc., Wallingford CT 2009.

[2] E. Runge, E.K.U. Gross, *Phys. Rev. Lett.* 1984, **52**, 997-1000.

[3] H. D. Cohen, C. C. J. Roothaan, *J. Chem. Phys.* 1965, **43**, S34-39.

[4] A. D. Buckingham, *Adv. Chem. Phys.* 1967, **12**, 107-142.

[5] Y. Li, Z. Li, D. Wu, R. Li, X. Hao, C. Sun, *J. Phys. Chem. B* 2004, **108**, 3145-3148.

[6] C. E. Dykstra, P. G. Jasien, *Chem. Phys. Lett*. 1984, **109**, 388-393.

[7] A. O. Lyakhov, A. R. Oganov, H. T. Stokes, Q. Zhu, Comput. *Phys. Commun.* 2013, **184,** 1172–1182.

[8] A. R. Oganov, C. W. Glass, *J. Chem. Phys.* 2006, **124**, 244704.

[9] A.R. Oganov, H. Stokes, M. Valle, *Acc. Chem. Res.* 2011, **44**, 227-237.

[10] G. Kresse, J. Furthmüller, *Phys. Rev. B*, 1996, **54**, 11169-11186.

[11] P. E. Blöchl, *Phys. Rev. B*, 1994, **50**, 17953.

[12] A. M. Rappe, K. M. Rabe, E. Kaxiras, J. D. Joannopoulos, *Phys. Rev. B* 1990, **41**, 1227-1230.

[13] J. P. Perdew, K. Burke and M. Ernzerhof, *Phys. Rev. Lett.*1996, **77**, 3865.

[14] S. J. Clark, M. D. Segall, C. J. Pickard, P. J. Hasnip, M. J. Probert, K. Refson, M. C. Z. Payne. *Kristallogr*. 2005, **220**, 567.

[15] C. Aversa, J. E. Sipe, *Phys. Rev. B* 1995, **52**, 14636-14645

[16] J. Lin, M. H. Lee, Z. P. Liu, C. T. Chen, C. J. Pickard. *Phys. Rev. B*. 1999, **60**, 13380.

[17] B. B. Zhang, M. H. Lee, Z. H. Yang, Q. Jing, S. L. Pan, M. Zhang, H. P. Wu, X. Su, C. S. Li, *Appl. Phys. Lett*. 2015, **106**, 031906.

[18] X. Gonze, B. Amadon, P. M. Anglade, J. M. Beuken, F. Bottin, P. Boulanger, F. Bruneval, D. Caliste, R. Caracas, M. Côté, T. Deutsch, L. Genovese, P. Ghosez, M. Giantomassi, S. Goedecker, D. R. Hamann, P. Hermet, F. Jollet, G. Jomard, S. Leroux, M. Mancini, S. Mazevet, M. J. T. Oliveira, G. Onida, Y. Pouillon, T. Rangel, G. M. Rignanese, D. Sangalli, R. Shaltaf, M. Torrent, M. J. Verstraete, G. Zerah, J. W. Zwanziger, *Comput. Phys. Commun*. 2009, **180**, 2582-2615.

[19] G. Kresse, J. Hafner, *Phys. Rev. B*. 1993, **47**, 558-561.

[20] S. Sharma, C. A.-Draxl, *Phys. Scr.* 2004, **T109**, 128-134,

[21] W. Jia, J. Fu, Z. Cao, L. Wang, X. Chi, W. Gao, L.- W. Wang, *J. Comput. Phys.* 2013, **251**, 102-115.

[22] M. Born and K. Huang, Dynamical theory of crystal lattices, Oxford University Press, 1998.

[23] R. Hill, *J. Mech. Phys. Solids,* 1963, **11**, 357–372.

[24] R. Hill, *Proc. Phys. Soc.* London, Sect. A, 1952, **65**, 349.

[25] X.-Q. Chen, H. Niu, D. Li, Y. Li, *Intermetallics*, 2011, **19**, 1275–1281.

[26] S. Pugh, London, Edinburgh Dublin Philos. Mag. J. Sci. 1954, **45**, 823–843.

[27] E. Mazhnik, A. R. Oganov, *J. Appl. Phys.* 2019, **126**, 125109.

[28] D. T. Morelli, G. A. Slack, High lattice thermal conductivity solids. High thermal conductivity materials. New York, USA: Springer; 2006. p. 37–68.

[29] D. R. Clarke, S. R. Phillpot, *Mater Today*, 2005, **8**, 22–9.

[30] J. Song, A. J. Freeman, T. K. Bera, I. Chung, M. G. Kanatzidis, *Phys. Rev. B*, 2009, **79**, 245203.

[31] M. Rérat, L. Maschio, B. Kirtman, B. Civalleri, R. Dovesi, *J. Chem. Theory Comput.* 2016, **12**, 107-113